

Journal of Biomedical Optics

SPIEDigitalLibrary.org/jbo

Altered lymphatic function and architecture in salt-induced hypertension assessed by near-infrared fluorescence imaging

Sunkuk Kwon
Germaine D. Agollah
Wenyaw Chan
Eva M. Sevick-Muraca

Altered lymphatic function and architecture in salt-induced hypertension assessed by near-infrared fluorescence imaging

Sunkuk Kwon,^a Germaine D. Agollah,^{ab} Wenyaw Chan,^c and Eva M. Sevick-Muraca^a

^aUniversity of Texas Health Science Center, Center for Molecular Imaging, The Brown Foundation Institute of Molecular Medicine, Houston, Texas 77030

^bUniversity of Texas Graduate School of Biomedical Sciences at Houston, University of Texas MD Anderson Cancer Center, Houston, Texas 77030

^cUniversity of Texas Health Science Center at Houston, School of Public Health, Houston, Texas 77030

Abstract. The lymphatic system plays an important role in maintaining the fluid homeostasis between the blood vascular and interstitial tissue compartment and there is recent evidence that its transport capabilities may regulate blood pressure in salt-induced hypertension. Yet, there is little known how the lymphatic contractile function and architecture responds to dietary salt-intake. Thus, we longitudinally characterized lymphatic contractile function and vessel remodeling noninvasively using dynamic near-infrared fluorescence imaging in animal models of salt-induced hypertension. The lymphatics of mice and rats were imaged following intradermal injection of indocyanine green to the ear tip or the base of the tail before and during two weeks of either a high salt diet (HSD) or normal chow. Our noninvasive imaging data demonstrated dilated lymphatic vessels in the skin of mice and rats on a HSD as compared to their baseline levels. In addition, our dynamic imaging results showed increased lymphatic contraction frequency in HSD-fed mice and rats. Lymphatic contractile function and vessel remodeling occurs in response to salt-induced hypertension suggesting a possible role for the lymphatics in the regulation of vascular blood pressure. © 2012 Society of Photo-Optical Instrumentation Engineers (SPIE). [DOI: 10.1117/1.JBO.17.8.080504]

Keywords: lymphatic contractile function; functional lymphatic imaging; near-infrared fluorescence imaging; salt; hypertension.

Paper 12252L received Apr. 23, 2012; revised manuscript received Jul. 10, 2012; accepted for publication Jul. 12, 2012; published online Aug. 16, 2012; corrected Aug. 21, 2012.

The hypothesis that primary or essential hypertension results from lymphatic system alteration has been suggested since 1998.¹ Although the precise mechanism for hypertension is largely unknown, dietary salt intake is considered as one of the major contributing factors to hypertension. Machnik et al.² demonstrated that vascular endothelial growth factor-C (VEGF-C), a major lymphangiogenic growth factor, is secreted by macrophages infiltrating the interstitium of the skin of mice

with 50% Swiss and 50% 129Sv genetic background and Sprague Dawley rats in response to a high salt diet (HSD). VEGF-C causes hyperplasia of lymphatic capillaries, thus resolving salt-induced hypertension, suggesting that the lymphatic system may play an important role in regulation of blood pressure. Additional evidence showed that extensive lymphatic fibrosis has been observed in the hearts of the Dahl salt-sensitive rats fed a HSD,³ indicating that hypertension induced by dietary salt can induce alteration of the lymphatic system. Since noninvasive, near-infrared fluorescence (NIRF) lymphatic imaging has been recently translated into the clinic,⁴ we sought to evaluate whether it can be used as a tool to evaluate lymphatic responses to salt-induced hypertension and antihypertensive therapies.

Recently, we have demonstrated for the first time, the ability to noninvasively image lymphatic drainage patterns and quantify lymphatic contractile function in normal healthy mice,⁵ tumor-bearing mice,⁶ and lymphedema-like phenotypic mice⁷ following intradermal (i.d.) injection of a NIR fluorescent dye, indocyanine green (ICG). However, it is unknown if/how lymphatic contractile function and remodeling can be changed during salt-induced hypertension. Therefore, we aimed to noninvasively and longitudinally image lymphatic function and remodeling in mice and rats fed a 4% and 8% HSD, respectively, using NIRF imaging to test our hypothesis that salt-induced hypertension is accompanied by changes in lymphatic contractile function and architecture.

Four to six weeks old male FVB mice ($n = 7$; Charles River, Wilmington, MA) and Sprague Dawley rats ($n = 9$; Charles River, Wilmington, MA) were housed and fed sterilized pelleted food and sterilized water. We imaged mice and rats in order to investigate if changes of lymphatic function due to salt-induced hypertension occur regardless of species. FVB mice were used since they have the most pronounced VEGF-C driven response to dietary salt (personal communication, Dr. Jens Titze). In addition, it was reported that VEGF-C induced lymphangiogenic response was higher in FVB mice compared with other strains, such as C57BL6 and Balb/c.⁸ All experiments were conducted according to protocols approved by the institutional Animal Welfare Committee (AWC), and in compliance with the American Association for Laboratory Animal Care.

During the two-week experimental period, five mice were fed a HSD (4% NaCl; Teklad Diets, Harlan Laboratories, Inc, Madison, WI) and 1% saline substituted for drinking water for two weeks, whereas two mice were given a normal diet pellets (Purina 5053, Labdiet PMI Nutritional International, St. Louis, MO) and sterilized water as control. Six Sprague Dawley rats received a HSD (8% NaCl; Teklad Diets, Harlan Laboratories, Inc, Madison, WI) and 1% saline as drinking water for two weeks. Another group of three rats received a normal diet and sterilized water for two weeks as control. Systolic blood pressure (SBP) was measured one day before NIRF imaging using a noninvasive tail-cuff method (CODA, Kent Scientific, Torrington, Connecticut) in conscious rats but not mice as the procedure induced stress related mortality in the FVB mice.

Animals were anesthetized with isoflurane and maintained at 37°C on a warming pad. In order to prevent fur from interfering with the fluorescent signal, animals were clipped 24 h before imaging. At each imaging session, dynamic NIRF imaging was performed immediately before and for up to 30 min after i.d. injection of 10 μ l or 50 μ l of 645 μ M of ICG (Akorn, Inc.,

Address all correspondence to: Sunkuk Kwon, University of Texas Health Science Center, Center for Molecular Imaging, The Brown Foundation of Molecular Medicine, 1825 Pressler Street, SRB 330F, Houston, Texas 77030. Tel: +713-500-3393; Fax: 713-500-0319; E-mail: Sunkuk.kwon@uth.tmc.edu

Lake Forest, IL) to the base of the mouse or rat tail, respectively, to image changes of lymphatic contractile function in response to dietary salt. Animals were imaged two to three times prior to the start of a HSD to establish baseline levels and every three to four days during a HSD for two weeks using a custom-built NIRF imaging system described elsewhere.⁷ Briefly, an animal was illuminated with 785 nm light from a laser diode outfitted with a convex lens, diffuser, and 785 nm bandpass filter to create a uniform excitation field. The 830 nm fluorescence was collected through holographic and bandpass filters placed prior to a 28 mm Nikon lens. The ears were also imaged using a macrolens following i.d. injection of 2 μ l of 645 μ M of ICG into the ear tip to image lymphatic capillary remodeling in response to a HSD. We used the concentration previously used in our animal studies.^{6,7,9} Animals in the control and experimental groups received the same ICG concentration and volume. The imaging data were analyzed with Matlab (The MathWorks, Inc., Natick, MA) and ImageJ (National Institutes of Health, Bethesda, MD) as described before.⁷ The same size of fixed regions of interest (ROIs) was defined along the entire fluorescent lymphatic vessels on fluorescence images. The averaged fluorescence intensity within each ROI in each fluorescence image was plotted as a function of distance and imaging time to generate a three-dimensional (3-D) spatio-temporal map. The number of pulses of ICG-laden lymph is an indication of lymphatic contractile activity and termed as contractions. The peak fluorescent intensities due to propagation of the fluorescent lymph along the lymphatic vessels were not influenced by respiration. The number of lymphatic contractions was measured for 5 min at 5 min after i.d. injection and the frequencies were calculated. The frequencies were normalized to the baseline, i.e., the data before any treatment. Fluorescent intensities in the draining inguinal LN (ILN), which can represent the extent of lymph flow, were also measured 10 mins after injection of ICG to mice. A circular ROI was selected over the inguinal region in control and treated mice and the averaged fluorescent intensity was measured. The ROI was the same size enabling comparison. Lymphatic diameters in rat ears after injection of 2 μ l of ICG were measured from the images of the ear using ImageJ software, since there is little scatter and lymphatic vessels are located at the surface (<1 mm in depth). Values are presented as means \pm the standard error of the mean (SEM). Statistical analysis was performed using SAS version 9.2 (SAS Institute Inc., Cary, NC). The data were analyzed using general linear model and the confidence interval for pairwise comparisons were calculated by Tukey's studentized range test. The *p*-value for each pairwise comparison was calculated from Fisher's least significant difference. The significance level was set at *p* < 0.05.

Rats were euthanized and ears and skin tissues were fixed in 10% formaldehyde and embedded in paraffin. Serial section slides were obtained from the paraffin-embedded specimens and stained with rabbit anti-mouse LYVE-1 (Angiobio, Del Mar, CA) primary antibody, secondary donkey antirabbit Alexa Fluor 546 (Invitrogen, Molecular Probes, Grand Island, NY), and Biostatus DRAQ5 (Enzo Life Sciences, Farmingdale, NY). Sections were viewed on a confocal Leica TCS SP5 fluorescent microscope (Leica Microsystems, Inc., Buffalo Grove, IL).

Previous data showed hyperplasia of lymphatic capillaries in the ear of mice and rats fed a HSD and 1% saline for drinking water, using *ex vivo* whole-mount or immunohistochemical (IHC) staining.² Our noninvasive imaging showed lymphatic drainage patterns in mice fed a HSD with i.d. injection of ICG to the

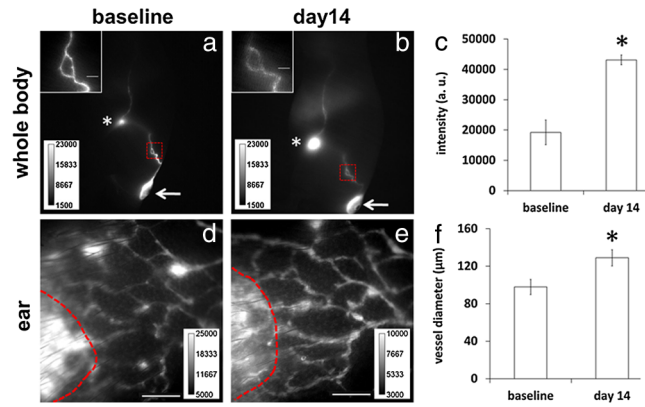


Fig. 1 Dilated lymphatic vessels were observed in the hindlimb [inset in (b)] of HSD-fed mice and in the ear of HSD-fed rats (e) as compared to baseline data in the hindlimb [inset in (a)] and in the ear (d). (c) Significantly increased fluorescent intensities in the ILN of HSD-fed mice were observed as compared to baseline. (f) The apparent average lymphatic vessel diameter associated with HSD was significantly enlarged as compared to baseline. *Inset*, magnified fluorescent images of the dashed rectangles. *Asterisk*, ILN. *Arrow*, ICG injection site. *Scale bar*: 1 mm. Dashed lines in (d) and (e) indicate the boundary of the injection site. * *p* < 0.05 versus baseline.

base of the tail did not change as compared to baseline. However, magnified fluorescent images using a macrolens revealed dilated lymphatic vessels in the limb of HSD-fed mice [Fig. 1(b)]. In addition, our data showed significantly increased fluorescent intensities in the ILN of HSD-fed mice as compared to baseline, indicating increased lymph flow [Fig. 1(c)]. Similar to these results in mice, our data also demonstrated dilated lymphatic vessels in the ear of rats fed a HSD [Fig. 1(f)], which were confirmed by immunofluorescence staining of lymphatic vessels (data not shown).

To unravel the effect of salt-induced hypertension on lymphatic contractile function, we conducted quantitative functional lymphatic imaging in mice and rats fed a HSD. Although previous studies to examine lymphatic contractile function have been done mainly in rats, there have not been any studies which have noninvasively characterized lymphatic function and drainage patterns in rats. Thus, we performed for the first time, noninvasive and dynamic imaging of the lymphatics in rats. Our imaging data demonstrated that lymphatic drainage pathways following i.d. injection of ICG to the base of the rat tail [Fig. 2(b) and video 1] are the same as shown in mice [Fig. 1(a) and 1(b)]. Although as in mice, our direct observation of the fluorescent images demonstrated that lymphatic drainage patterns did not change in response to a HSD. The SBP in rats fed a HSD for a week was significantly higher than baseline and that in control rats (143 \pm 2 versus 117 \pm 2 mm Hg, respectively). HSD feeding in rats for two weeks did not significantly increase blood pressure as compared to rats fed a HSD for one week (141 \pm 2 versus 143 \pm 2 mm Hg, respectively).

In order to elucidate whether lymphatic contractility is affected in response to salt-induced hypertension, the frequency of contractions were measured. ROIs were selected along fluorescent lymphatic vessels [Fig. 2(b)] and fluorescent intensities as a function of time and ROI were plotted. As shown in 3-D spatio-temporal maps [Fig. 2(c) and 2(d)], the maximum intensity indicates waves of ICG-laden lymph movement along the internodal collecting lymphatic vessels. Mice fed a HSD for a week showed an increase in the frequency of contractions in the

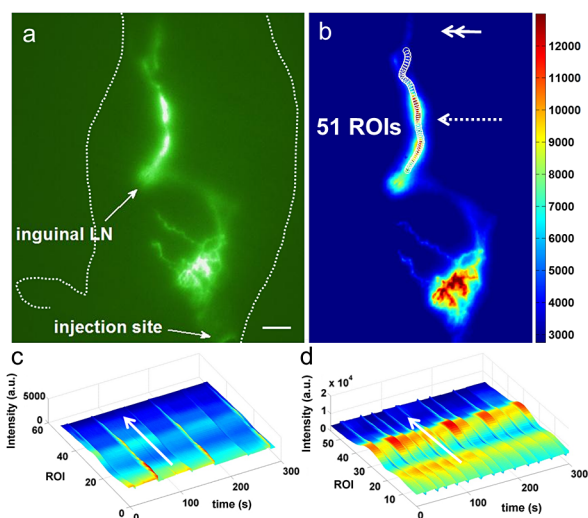


Fig. 2 Fluorescent images (a) and (b) in the left lateral view of a rat showing lymphatic trafficking of ICG-labeled lymph from the injection site to the ILN and subsequently to the axillary LN (double arrow) via the internodal collecting lymphatic vessels (broken arrow) where 51 circular ROIs (12 pixels in radius) were selected (Video 1, MOV, 5 MB) [DOI: <http://dx.doi.org/10.1117/1.JBO.17.8.080504.1>]. The video shows a series of static fluorescent images depicting propulsive lymph flow in rats 14 days after a HSD and 1% saline as drinking water. Scale bar: 1 cm. (c) and (d) A 3-D plot of fluorescent intensity as a function of time and ROI shows more propagating contraction waves (d) in rats fed a HSD for two weeks as compared to baseline (c). Arrow, propagation of the fluorescent lymph along the lymphatic vessels.

inguinal afferent (from the injection site to the ILN) and efferent (from the ILN to the ALN) lymphatic vessels to $147 \pm 19\%$ and $156 \pm 19\%$, respectively, of the baseline and the frequencies were further increased to $206 \pm 24\%$ and $191 \pm 18\%$, respectively, of the baseline at 14 days after a HSD [Fig. 3(a) and 3(b)]. Similar patterns were also observed in HSD-fed rats. Feeding a HSD for one and two weeks caused an increase in the frequency of contractions in afferent lymphatic vessels to $145 \pm 33\%$ and $278 \pm 99\%$, respectively, of the baseline [Fig. 3(c)]. The frequency of contractions in the inguinal efferent lymphatic vessels of rats on the HSD significantly increased to $149 \pm 32\%$ and $198 \pm 14\%$ of the baseline after 7 and 14 days, respectively. The baseline data were not significantly different from those in control mice and rats (Fig. 3).

In this study, we have demonstrated the proof of concept that salt-induced hypertension can induce functional and architectural changes of the lymphatic system. Previous data showed VEGF-C secretion by macrophages in the skin of mice and rats fed a HSD is responsible in part for ameliorating salt-induced hypertension.² VEGF-C, a major lymphangiogenic growth factor,¹⁰ induced hyperplastic lymphatic capillaries, thus possibly resulting in increased lymph flow. However, there have not been any studies to noninvasively show whether architectural changes in functional lymphatics occur because of salt-induced hypertension. Our data from noninvasive, functional lymphatic imaging demonstrated dilated lymphatic vessels and significantly increased lymphatic contractility in mice and rats fed a HSD. Previously, Breslin et al.¹¹ showed that VEGF-C and a VEGFR-3-specific mutant form of VEGF-C, VEGF-C156S, significantly increased lymphatic contraction frequency and end-diastolic diameter in a time-dependent manner in normal rat mesenteric collecting lymphatics observed in situ by intravital microscopy. Therefore, VEGF-C may play an important role not only in formation of

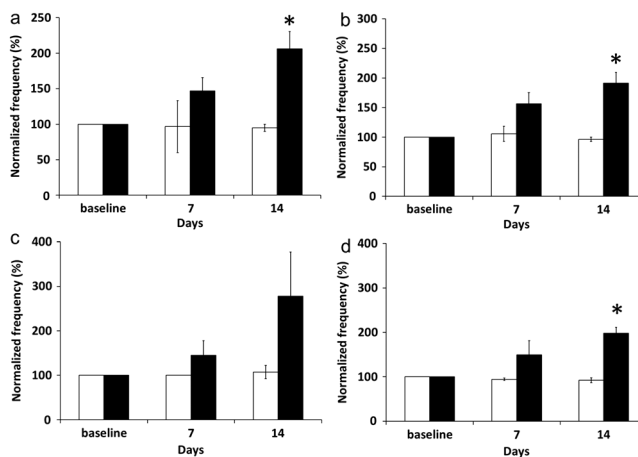


Fig. 3 Increased lymphatic contraction frequency in the inguinal afferent (a) and (c) and efferent (b) and (d) lymphatic vessels in HSD-fed (black bars) mice (a) and (b) and rats (a) and (d) as compared to controls (white bars) and baseline. * $p < 0.05$ versus control.

new lymphatic vessels i.e., lymphangiogenesis, and maintenance of a lymphatic network, but also in the physiological regulation of lymphatic contractility.

In conclusion, the work presented herein provides preclinical evidence for the use of the novel NIRF imaging technology for evaluating lymphatic response in animal models of hypertension. If translated, the imaging approach could provide a new companion diagnostic for evaluating therapeutic response of antihypertensive agents, which often cause peripheral edema in patients, and other emerging therapeutics that ameliorate hypertension.

Acknowledgments

This work was supported in parts by NIH R01 HL092923-04 and the Texas Star Award. We thank Gabriel Dickinson, Pier-Anne Lachance, Holly Robinson, and Karen Gore for their technical assistance.

References

1. J. E. Mekarski, "Essential hypertension is lymphatic: a working hypothesis," *Med Hypotheses*. **51**(2), 101–103 (1998).
2. A. Machnik et al., "Macrophages regulate salt-dependent volume and blood pressure by a vascular endothelial growth factor-C-dependent buffering mechanism," *Nature Med.* **15**(5), 545–552 (2009).
3. X. Li et al., "Ultrastructure changes of cardiac lymphatics during cardiac fibrosis in hypertensive rats," *Anat. Rec.* **292**(10), 1612–1618 (2009).
4. E. M. Sevick-Muraca, "Translation of near-infrared fluorescence imaging technologies: emerging clinical applications," *Annu. Rev. Med.* **63**, 217–231 (2012).
5. S. Kwon and E. M. Sevick-Muraca, "Noninvasive quantitative imaging of lymph function in mice," *Lymphat. Res. Biol.* **5**(4), 219–231 (2007).
6. S. Kwon and E. M. Sevick-Muraca, "Functional lymphatic imaging in tumor-bearing mice," *J. Immunol. Methods*. **360**(1–2), 167–172 (2010).
7. S. Kwon and E. M. Sevick-Muraca, "Mouse phenotyping with near-infrared fluorescence lymphatic imaging," *Biomed. Opt. Express* **2**(6), 1403–1411 (2011).
8. B. Regenfuss et al., "Genetic heterogeneity of lymphangiogenesis in different mouse strains," *Am. J. Pathol.* **177**(1), 501–510 (2010).
9. P. E. Lapinski et al., "RAS1 maintains the lymphatic vasculature in a quiescent functional state in mice," *J. Clin. Invest.* **122**(2), 733–747 (2012).
10. K. Alitalo and P. Carmeliet, "Molecular mechanisms of lymphangiogenesis in health and disease," *Cancer Cell*. **1**(3), 219–227 (2002).
11. J. W. Breslin et al., "Vascular endothelial growth factor-C stimulates the lymphatic pump by a VEGF receptor-3-dependent mechanism," *Am. J. Physiol. Heart Circ. Physiol.* **293**(1), H709–718 (2007).